

Supersolidity, entropy, and frustration: t - t' - V model of hard-core bosons on the triangular lattice

S. R. Hassan,¹ L. de Medici,² and A.-M. S. Tremblay¹

¹*Department de Physique and RQMP, Université de Sherbrooke, Sherbrooke, Québec, Canada J1 K 2R1*

²*Department of Physics and Center for Materials Theory, Rutgers University, Piscataway, New Jersey 08854, USA*

(Received 5 September 2007; published 16 October 2007)

We study the properties of t - t' - V model of hard-core bosons on the triangular lattice that can be realized in optical lattices. By mapping to the spin-1/2 XXZ model in a field, we determine the phase diagram of the t - V model where the supersolid characterized by the ordering pattern $(x, x, -2x')$ (“ferrimagnetic” or SS A) is a ground state for chemical potential $\mu > 3V$. By turning on either temperature or t' at half filling ($\mu = 3V$), we find a first order transition from SS A to the elusive supersolid characterized by the $(x, -x, 0)$ ordering pattern (“antiferromagnetic” or SS C). In addition, we find a large region where a superfluid phase becomes a solid upon increasing temperature at fixed chemical potential. This is an analog of the Pomeranchuk effect driven by the large entropic effects associated with geometric frustration on the triangular lattice.

DOI: [10.1103/PhysRevB.76.144420](https://doi.org/10.1103/PhysRevB.76.144420)

PACS number(s): 75.10.Jm, 05.30.Jp, 67.40.Kh, 74.25.Dw

I. INTRODUCTION

Supersolidity is one of the most intriguing properties of matter. In that state, matter can flow without viscosity, like in a superfluid, yet atoms are located at regular positions: Translation and U(1) symmetry are broken simultaneously. It was originally proposed¹ that this state could exist in ⁴He. While such a supersolid state may have been observed,² it is likely that the relevant mechanism for ⁴He is disorder,³ not zero point vacancies as first envisioned.

To observe supersolidity without disorder, one can load ultracold bosonic atoms into optical lattices.⁴ Indeed, Bose-Einstein condensation of chromium atoms in an optical trapping potential⁵ has already been observed, making it likely that supersolid phases on such lattices can eventually be achieved. Temperature is clearly an extremely relevant parameter for these experiments.⁶

One of the most promising lattices to observe supersolid phases is the triangular lattice where supersolidity appears as a result of geometric frustration, from a kind of order-by-disorder mechanism.⁷⁻¹¹ Supersolidity in other two-dimensional lattice models has been predicted theoretically, but the triangular lattice offers a particularly rich and interesting phase diagram in a lattice that is simple to realize. For example, it has been proposed¹² that second-neighbor hopping may induce the intriguing particle-hole symmetric supersolid C phase, (the so-called antiferromagnetic supersolid). It has been conjectured¹³ that the transition between supersolid C and other phases, such as supersolid A (“ferrimagnetic” supersolid), could occur through a critical point with emergent degrees of freedom that cannot be described by the standard Landau theory.¹³

In this paper, we obtain detailed phase diagrams showing that a particle-hole symmetric supersolid phase C can indeed be stabilized by both next-nearest-neighbor hopping and by finite-temperature effects. In addition, the frustration associated with the triangular lattice amplifies entropic effects, leading to a wide range of parameters where one can observe superfluid-solid-liquid transitions as temperature is increased at constant chemical potential. On the square lattice,¹⁴ this sequence of transitions occurs in an extremely narrow range

of chemical potentials. This phenomenon is an analog of the Pomeranchuk effect in ³He, where liquid (not superfluid)-solid-liquid transitions are observed by increasing T at fixed pressure.

II. MODEL AND METHOD

We consider hard-core bosons (infinite on-site repulsion) on a triangular lattice, with both nearest-neighbor hopping and repulsion (t, V) and next-nearest-neighbor hopping (t'),

$$H = - \sum_{i,j} t_{ij} a_i^\dagger a_j + \text{H.c.} + V \sum_{\langle ij \rangle} n_i n_j - \mu \sum_i n_i, \quad (1)$$

where each lattice site can be occupied by 0 or 1 boson ($n_i = 0, 1$), $n_i = a_i^\dagger a_i$, and μ is the chemical potential. In the above restricted Hilbert space, the model (1) can be mapped to the $S=1/2$ XXZ model in a field (h),

$$\mathcal{H} = V \sum_{\langle ij \rangle} S_i^z S_j^z - \sum_{i,j} t_{ij} S_i^- S_j^+ + \text{H.c.} - h \sum_i S_i^z, \quad (2)$$

where $h = \mu - 3V$. In this language, supersolid (SS) ordering corresponds to spins having their x - y component aligned ferromagnetically [superfluid (SF)] along with their z component also ordered but at nonzero wave vector inside the first Brillouin zone [solid (S)]. A phase without ordering but nonzero z component and zero x - y component corresponds to the normal fluid (NF). Fully polarized up (down) spins corresponds to full (empty) lattice. The order parameter for the solid (staggered magnetization in spin language, staggered density in boson language) is defined with the help of the three sublattice magnetizations ($S_i^z = n_i - 1/2, i=1, 2, 3$) as¹⁵ $M_s = \sqrt{3[(S_1^z)^2 + (S_2^z)^2 + (S_3^z)^2 - S_1^z S_2^z - S_1^z S_3^z - S_2^z S_3^z]}$. It measures the solid order, i.e., a periodicity longer than that of the underlying lattice.

The Berezinskii-Kosterlitz-Thouless (BKT) transitions and the SS C phase (in the $t/V \rightarrow 0$ limit)⁶ are normally out of reach for simple mean-field theories. Using large enough clusters, however, self-consistent cluster mean-field theory (SCMFT) can overcome some of these deficiencies. We argue that, while not perfectly accurate, SCMFT¹⁶ is an extremely efficient way of exploring vast uncharted territory in

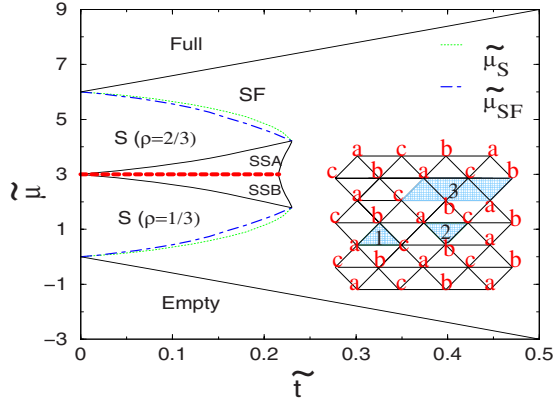


FIG. 1. (Color online) Zero-temperature phase diagram for the triangular lattice. Second order phase transitions are denoted by solid lines, whereas $\tilde{\mu}_S$ and $\tilde{\mu}_{SF}$ are spinodal lines as a function of inverse coupling strength $\tilde{t}=t/V$. The thick dashed lines at $\tilde{\mu}=3$ indicate first order transition between SS A to SS B. Inset shows $\sqrt{3} \times \sqrt{3}$ ordering of the solid and supersolid phases.

the phase diagram. More refined studies can then improve the accuracy of phase boundaries in a second stage. We briefly describe the method and then demonstrate its accuracy by comparing with known results.

A cluster “1” with a finite number of sites (shaded region of the inset of Fig. 1) is embedded in the effective field of its surroundings. (Cluster shapes are chosen to respect lattice symmetry.) In other words, we consider the following cluster \mathcal{C} spin Hamiltonian \mathcal{H}_s :

$$\mathcal{H}_s = \sum_{i,j \in \mathcal{C}} \mathcal{H}_{ij} + \sum_{i \in \mathcal{C}} h_i^- S_i^+ + \text{H.c.} + \sum_{i \in \mathcal{C}} h_i^z S_i^z - h \sum_{i \in \mathcal{C}} S_i^z, \quad (3)$$

where h_i^- and h_i^z are the effective fields of the surroundings. \mathcal{H}_s needs to be diagonalized with the following self-consistency conditions:

$$h_i^{-/+} = \sum_j' t_{ij} \langle S_j^{\mp/+} \rangle, \quad h_i^z = \sum_j' V_{ij} \langle S_j^z \rangle, \quad (4)$$

where j indicates neighbor of site i and prime over Σ indicates that sites j inside the cluster are excluded. Average values in Eq. (4) are obtained from \mathcal{H}_s .

III. VALIDITY OF THE APPROACH

To assess the accuracy of SCMFT, we first show that it reproduces quite accurately the phase diagram obtained from the most reliable approaches. From now on, we discuss the results mostly in the bosonic language. For the t - V model, consider a cluster “1” of three sites shown as a shaded area in the inset of Fig. 1. We measure t , μ , and temperature T in units of V , defining $\tilde{t}=t/V$, $\tilde{\mu}=\mu/V$, and $\tilde{T}=T/V$.

We display the zero-temperature phase diagram in Fig. 1. This phase diagram is very close to the phase diagram obtained by quantum Monte Carlo (QMC) methods in Refs. 6 and 7. In the simplest mean-field approach,¹⁷ the supersolid region at $\tilde{\mu}=3$ is much too large, extending to $(\tilde{t})^{MF}=0.5$ compared with $(\tilde{t})^{QMC}=0.124$ in Ref. 7. Here, we obtain

0.216, closer to QMC. Also, in our approach, the maximum extent of the solid region, $\tilde{t}=0.22$, is overestimated by only 10% compared with the QMC result 0.195. In Fig. 1, we show the spinodals $\tilde{\mu}_S(\tilde{t})$ and $\tilde{\mu}_{SF}(\tilde{t})$ between which metastable phases or coexistence of SF and S may occur.

In supersolid A (SS A, $\tilde{\mu}>3$), the density on three consecutive sites follows the ferrimagnetic ordering patterns $\langle n_i - \frac{1}{2} \rangle = \langle S_i^z \rangle = (x, x, -2x')$. In supersolid B (SS B, $\tilde{\mu}<3$), the pattern is $(-x, -x, 2x')$ with $x \neq x'$. This pattern is the same as that in Refs. 6 and 8, in contrast with $x=x'$ found in Ref. 7. The density has a discontinuous jump at $\tilde{\mu}=3$; hence, the SS A–SS B transition is first order. Larger cluster size (nine sites) confirms this result. All these results (and more below) validate the SCMFT approach to the hard-core boson problem. The spinodal lines $\tilde{\mu}(\tilde{t})$ for the supersolid phases (not shown) have roughly a parabolic shape, closing at the critical end points $(\tilde{\mu}=3, \tilde{t}=0)$ and $(\tilde{\mu}=3, \tilde{t}_c=0.216)$, the latter being the SS to SF transition. The maximum size of the metastable region, $\tilde{\mu}=\pm 3.01$, occurs halfway between $\tilde{t}=0$ and \tilde{t}_c .

The main properties of the supersolid phases are summarized as follows at the particle-hole symmetric point $\tilde{\mu}=3$ (half filling). When \tilde{t} approaches 0, the supersolid state is in close proximity to the insulating states $\rho=2/3$ ($\rho=1/3$); therefore, the jump in density $\delta\rho$ is maximum in this region. The staggered density M_s is also maximum there and vanishes continuously at the critical point $\tilde{t}_c=0.216$ after which only superfluidity survives. The superfluid density ρ_s corresponds to the spin stiffness in spin language. It measures the energy cost to introduce a twist θ of the direction of spin between every pair of neighboring rows. We use its generalization to finite temperature following Ref. 18. The SS A to SF transition is a continuous quantum phase transition with a kink in ρ_s at the transition point. The value of ρ_s that we find there (0.18) is within a few percent of the QMC results.⁷

IV. FINITE-TEMPERATURE PHASE DIAGRAM AT FINITE DOPING

In Fig. 2, we present the finite-temperature phase diagram along a vertical line $\tilde{t}=0.1$ of Fig. 1. Because of particle-hole (Ising) symmetry, it is sufficient to show $\tilde{\mu} \geq 3$. Over a wide range of chemical potentials at high temperatures, a first order S to NF phase transition (dashed line) ends at a tricritical point **d** at about $\tilde{\mu}=3.70$, where second order melting transition of the solid begins. Point **e** at the other end of the first order line marks the beginning of a very interesting region at large $\tilde{\mu}$. The first order transition bifurcates: to the right into a (BKT) transition separating SF and NF and to the left into a first order transition separating SF and S. Between point **e** and point **f**, we find the remarkable sequence of phases described in the Introduction: As we increase the temperature at fixed $\tilde{\mu}$, one encounters SF, S, then NF. The superfluid solidifies as we increase temperature because of an analog of the Pomeranchuk effect, the role of spin entropy being played by hard-core boson occupation of optical lattice sites. Solidification does not quench all the entropy. Let us come back to the BKT transition to the right of point **e**. One does expect the SF to NF transition to be of this nature.¹⁴ Clearly,

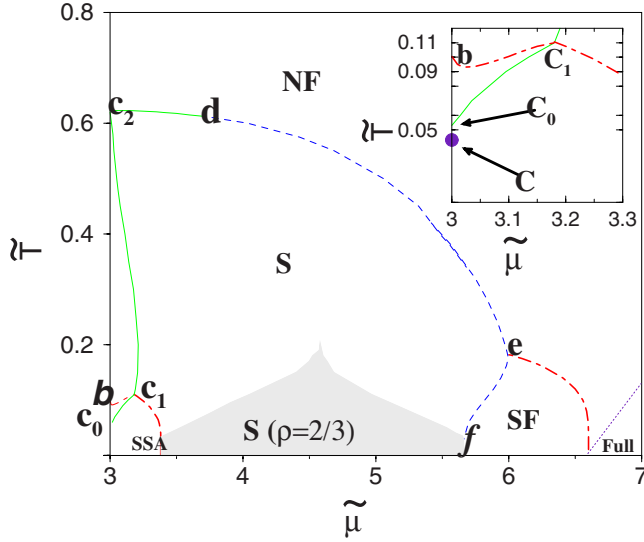


FIG. 2. (Color online) (a) $\tilde{\mu}$ - \tilde{T} Phase diagram corresponding to a vertical line $\tilde{T}=0.1$ in Fig. 1. The inset shows the behavior near the particle-hole symmetric point $\tilde{\mu}=3$. The two arrows indicate the region of metastability of supersolid phases between \tilde{T}_{c_0} and \tilde{T}_c .

SCMFT cannot accurately describe the topological BKT transition. Nevertheless, we take the jump in superfluid density ρ_s illustrated in the inset of Fig 4, and the continuous vanishing of the order parameter $\Psi \equiv \langle S_x \rangle = \langle (b + b^\dagger) / 2 \rangle$ as very clear SCMFT signatures of the BKT transition.

Supersolid phases appear near the symmetric point $\tilde{\mu}=3$. For $\tilde{\mu} \leq 3.38$, the solid freezes into various supersolid phases with decreasing temperature. For example, at $\tilde{\mu}=3.2$, the staggered density M_s and the density ρ change continuously from S to the finite $\tilde{\mu}$ extension of SS A, but again there is a jump in the ρ_s , as shown the inset of Fig. 4, so the transition is of the BKT type.

The inset in Fig. 2 is a blowup of the region around the particle-hole symmetric point $\tilde{\mu}=3$, where supersolid phases appear. At $\tilde{\mu}=3$, increasing \tilde{T} from zero, we notice that the ordering pattern of the solid changes from ferrimagnetic SS A $(x, x, -2x')$ to antiferromagnetic SS C $(x, -x, 0)$ at $\tilde{T}_{c_0} = 0.053$, indicated by point c_0 in the inset. The SS A to SS C transition is first order, as can be seen from the hysteresis in the plot of density as a function of \tilde{T} in Fig. 3(a). The region of metastability associated with this transition is in the range $\tilde{T}_c (=0.043) < \tilde{T} < \tilde{T}_{c_0}$. The SS C phase continues to higher temperature, up to point **b**. The SS C to solid transition point **b** (of BKT type) is indicated by the second arrow in Fig. 3(a). The area delimited by c_0 - c_1 -**b** contains the ferrimagnetic $(x, -x', x'')$ supersolid phase that evolves from SS C with increasing $\tilde{\mu}$ for $\tilde{T}_{c_0} < \tilde{T} < \tilde{T}_b$. The c_0 - c_1 line is second order. Dependence on $\tilde{\mu}$ at fixed $\tilde{T}=0.06$ for the superfluid order parameter and the density is shown in Fig. 3(b). The arrow to the right indicates the BKT transition from SS A to S: In Ref. 6, a BKT transition from SS A to S was also found with QMC at very similar temperatures. The arrow to the left marks the transition from SS C to SS A. The region **b**- c_1 - c_2

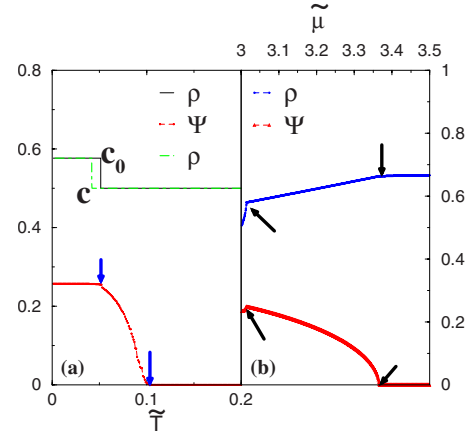


FIG. 3. (Color online) (a) Density (ρ), hysteresis, and superfluid order parameter (Ψ) as a function of \tilde{T} along the $\tilde{\mu}=3$ vertical line of the phase diagram in Fig. 2. (b) Same quantities but this time as a function of $\tilde{\mu}$ along the horizontal line $\tilde{T}=0.06$ in the phase diagram of Fig. 2.

delineates the solid order that evolves from a $(x, -x, 0)$ pattern. Outside this region, the solid phase has ordering $(x, x, -x')$, and the transition between the two types of solids is second order.

The plot of density as a function of $\tilde{\mu}$ in Fig. 4 confirms the order of the last two transitions we mentioned. The first kink in the $\tilde{T}=0.4$ and that in the $\tilde{T}=0.09$ curves are associated with, respectively, the second order solid to solid and SS C to SS A (at finite $\tilde{\mu}$ where both phases are ferrimagnetic).

V. FINITE SECOND-NEIGHBOR HOPPING t'

Finally, we investigate whether second-neighbor hopping t' , in the particle-hole symmetry case $\tilde{\mu}=3$, can induce the SS C phase at zero temperature, as proposed in Ref. 12. A finite t' allows same sublattice hopping. In the presence of t' , we choose clusters “1” and “2” shown in the inset of Fig. 1

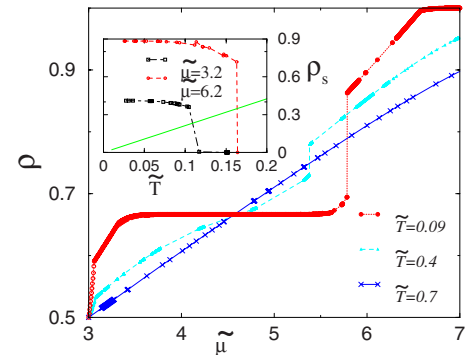


FIG. 4. (Color online) Density as a function of $\tilde{\mu}$ for various values of \tilde{T} , each of which corresponds to a different horizontal cut on the phase diagram of Fig. 2. The inset shows the BKT transition in ρ_s as a function of \tilde{T} at $\tilde{\mu}=3.2$ and 6.2 . The straight diagonal line is the BKT prediction.

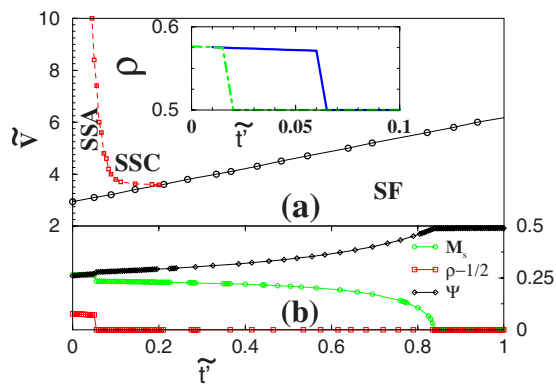


FIG. 5. (Color online) (a) The ground-state phase diagram for the t - t' - V model at $\tilde{\mu}=3^+$. The solid line indicates second order transition, whereas broken line indicates the first order transition. t' and V are measured with respect to t . The inset shows ρ vs t' hysteresis curve at $\tilde{V}=6$. (b) M_s , $\rho-1/2$, and Ψ as a function of t' for $\tilde{V}=6$.

and connect them to each other through the perturbation t' . The effects of the other bonds that connect clusters “1” and “2” are included in the self-consistent Eq. (4). We checked that the ground-state energy of this cluster is lower than that of cluster “3” (where all bonds reside on the cluster).

The ground-state phase diagram for $\tilde{\mu}=3^+$ is shown in Fig. 5(a). We note that for $\tilde{V}=V/t > 3.0$, a small value of the perturbation $\tilde{t}'=t'/t$ drives SS A to SS C through a strong first order transition, as can be seen from the hysteresis exhibited in the inset of Fig. 5(a). In part (b) of the same figure, we plot the staggered density M_s , the superfluid order parameter Ψ , and the average value of $\rho-1/2$ as a function of \tilde{t}' at $\tilde{\mu}=3$, corresponding to a horizontal cut at $\tilde{V}=6$ in the phase diagram. We note that the finite value of $\rho-1/2$ corresponds to SS A. With increasing \tilde{t}' , the value of $\rho-1/2$ jumps to zero, indicating SS C. Similar jumps can be seen in the other two curves.

VI. CONCLUSION AND SUMMARY

In summary, the strong geometric frustration present on the triangular lattice has striking consequences on the phase diagram of hard-core bosons. First, as is well known, it allows the ferrimagnetic SS A and SS B phases to appear at $T=0$. Second, the triangular lattice is associated with strong entropic effects at finite T that, as we have shown, lead to a pronounced Pomeranchuk effect. We have also shown at the particle-hole symmetric point $\tilde{\mu}=3$ that entropic effects at finite T , or finite t' at $T=0$, lead to the appearance of the elusive antiferromagnetic SS C phase. Since the SS A and SS B supersolids break particle-hole symmetry, it is natural that increasing temperature restores a symmetric SS C state. In the case of t' , it is a simple exercise to show that for same sublattice hopping, kinetic energy is minimized by $(|0\rangle + |1\rangle)/\sqrt{2}$, i.e., the 0 state in spin language. Finite t' thus also favors the restoration of the SS C $(x, -x, 0)$ state. The SS A to SS C transition is strongly first order under the influence of either T or t' at $\tilde{\mu}=3^+$. It is clearly not possible to see non-Landau quantum critical point¹³ with SCMFT; nevertheless, it is likely that transitions that are strongly first order in SCMFT will not become continuous unless quantum fluctuations beyond the cluster size are singular enough to completely drive the transition. This is a delicate point that requires much more detailed studies guided by our results for phase boundaries. Our finite-temperature results are important for experimental studies of this very rich phase diagram with optical lattices or in solid state XXZ spin analogs.

ACKNOWLEDGMENTS

S.R.H. thanks A. Georges and R. Moesner for stimulating discussions at the initial stage of the project. We also thank M. Boninsegni, B. Davoudi, B. Kyung, A. H. Nevidomskyy, A. Paramekanti, and N. Prokof'ev for useful conversations. Computations were performed on the Ms RQCHP cluster. The present work was supported by NSERC (Canada), CFI (Canada), CIAR, the Tier I Canada Research Chair Program (A.-M.S.T.), and the Center for Materials Theory, Rutgers University (L.d.M.).

¹A. Andreev and I. Lifshitz, Sov. Phys. JETP **29**, 1107 (1969); G. Chester, Phys. Rev. A **2**, 256 (1970); A. J. Leggett, Phys. Rev. Lett. **25**, 1543 (1970).
²E. Kim and M. H. W. Chan, Nature (London) **427**, 225 (2004).
³P. Phillips and Alexander V. Balatsky, Science **316**, 1435 (2007).
⁴L.-M. Duan, E. Demler, and M. D. Lukin, Phys. Rev. Lett. **91**, 090402 (2003).
⁵A. Griesmaier, Jörg Werner, Sven Hensler, J. Stuhler, and Tilman Pfau, Phys. Rev. Lett. **94**, 160401 (2005).
⁶M. Boninsegni and N. Prokofev, Phys. Rev. Lett. **95**, 237204 (2005).
⁷S. Wessel and M. Troyer, Phys. Rev. Lett. **95**, 127205 (2005).
⁸D. Heidarian and K. Damle, Phys. Rev. Lett. **95**, 127206 (2005).
⁹R. G. Melko, A. Paramekanti, A. A. Burkov, A. Vishwanath, D. N. Sheng, and L. Balents, Phys. Rev. Lett. **95**, 127207 (2005).
¹⁰J. Oitmaa, Weihong Zheng, and D. Tompsett, Phys. Rev. B **73**,

172401 (2006).

¹¹R. G. Melko, A. Del Maestro, and A. A. Burkov, Phys. Rev. B **74**, 214517 (2006).

¹²A. A. Burkov and L. Balents, Phys. Rev. B **72**, 134502 (2005).

¹³T. Senthil, L. Balents, S. Sachdev, A. Vishwanath, and M. P. A. Fisher, Science **303**, 1490 (2004); Phys. Rev. B **70**, 144407 (2004).

¹⁴G. Schmid, Synge Todo, Matthias Troyer, and Ansgar Dorneich, Phys. Rev. Lett. **88**, 167208 (2002).

¹⁵J. Richter, D. J. J. Farnell, R. F. Bishop, in *Quantum Magnetism*, edited by U. Schöllwock, Lecture Notes in Physics Vol. 645 (Springer-Verlag, Berlin, 2004), pp. 85–153.

¹⁶E. Zhao and A. Paramekanti, arXiv:0706.2657 (unpublished).

¹⁷G. Murthy, D. Arovas, and A. Auerbach, Phys. Rev. B **55**, 3104 (1997).

¹⁸X. Zotos and P. Prelovsek, Phys. Rev. B **53**, 983 (1996).